Electroconvection with and without the Carr-Helfrich effect in a series of nematics

Elżbieta Kochowska[1,*], Szilárd Németh[1], Gerhard Pelzl[2] and Ágnes Buka[1]

[1]Research Institute for Solid State Physics and Optics,

Hungarian Academy of Sciences,

H-1525 Budapest, P.O.B.49, Hungary

e-mail:kochowsk@power.szfki.kfki.hu

[2] Institut für Physikalische Chemie,

Martin Luther Universität,

D-06099 Halle/Saale, Germany

Experimental electroconvection investigations on four homologs with negative dielectric anisotropy ε_a and conductivity anisotropies σ_a of various signs (the relative $\hat{\sigma}_a = \frac{\sigma_a}{\sigma_\perp}$ ranges from -0.6 to +0.3) are reported. The homolog with positive conductivity anisotropy follows the predictions of the standard theoretical model, while the homolog with negative σ_a shows a new phenomenon i.e. non-standard electroconvection, not described by the Carl-Helfrich mechanism but manifesting in forms of stripes mainly parallel to the initial director thus having morphological similarity to the rolls of the standard EC. The remaining two homologs change the sign of their conductivity anisotropy with temperature that leads to a twofold character by crossing over from standard to non-standard electroconvection. Both the rolls of the standard electroconvection and the stripes of the non-standard case have been characterized and compared.

I.   INTRODUCTION

It is well known that systems far from equilibrium can create a great variety of patterns [1, 2]. Electro-hydrodynamic convection (EC) in liquid crystals has proved to be a useful system for studies of pattern formation in non-equilibrium systems due to the inherent anisotropy and the easy control of the external parameters.

In nematics the mean orientation of the molecules is described by the director $\mathbf{n}$. The anisotropic features are reflected in the material parameters, such as the conductivity σ_{ij} and the dielectric permittivity tensor ε_{ij}. Using the expression $\sigma_a = \sigma_\parallel - \sigma_\perp$ for the conductivity anisotropy one has: $\sigma_{ij} = \sigma_\perp \delta_{ij} + \sigma_a n_i n_j$, where $\parallel$ ($\perp$) denotes the conductivity measured parallel (perpendicular) to $\mathbf{n}$,

---

* On leave from Henryk Niewodniczanski Institute of Nuclear Physics, Polish Academy of Sciences, PL 31-342
  Krakow, Poland

and similarly $\varepsilon_{ij} = \varepsilon_\perp \delta_{ij} + \varepsilon_a n_i n_j$ with $\varepsilon_a = \varepsilon_\parallel - \varepsilon_\perp$. Other material parameters, e.g. the elasticity and viscosity are also anisotropic, however, their symmetry differs from that of ε_{ij} and σ_{ij} [3, 4].

The value, the sign and that of their anisotropies of the material parameters, in particular the sign of ε_a and σ_a is decisive for EC.

In order to categorize substances concerning their EC behavior a system of notations $(-+)$ $(+-)$ $(++)$ and $(--)$ was introduced, where the first sign labels the sign of ε_a and the second one that of σ_a. EC was theoretically predicted to occur via the *Carr-Helfrich* mechanism for the first two and prohibited for the last two cases [3]. More detailed studies (the 3D standard model of EC [5]) revealed a finer picture particularly in the vicinity of $\varepsilon_a = 0$ and/or $\sigma_a = 0$. The linear EC threshold based on the Carr-Helfrich mechanism does not necessarily appear/dissapear exactly at the sign inversion of ε_a or σ_a. Instead, the EC stability region either persists up to a small value of the opposite sign of the parameter, or it terminates before the anisotropy reaches zero. This means e.g. in the most studied planar $(-+)$ case that on the one hand, keeping $\sigma_a > 0$ EC actually occurs for all $\varepsilon_a \le 0$ and up to a small positive value of ε_a given by the condition where the EC threshold voltage becomes equal to the splay Frèedericksz threshold, thus the EC stability region labeled by $(-+)$ penetrates into the $(++)$. On the other hand, keeping $\varepsilon_a < 0$ and decreasing σ_a, EC disappears before σ_a reaches zero (for details see later in this paper). Keeping in mind the above corrections to the classical description we still use the above notation for convenience.

In the $(-+)$ case (such as MBBA [5–8], Phase5A(Merck) [9–12], I52 [13] or Phase4 [14]) EC is a well-investigated phenomenon, theory and experimental results fit well. Some of the recent observations have focused on materials with opposite signs $(+-)$ of the anisotropies [15], where the *standard model* [5] gives a good qualitative and quantitative description, too. The recently studied $(++)$ case for small, positive ε_a is characterized by a competition between a static distortion (Frèedericksz state) and EC [16]. This then behaves identically in the EC state to substances in the category $(-+)$.

In this work we consider materials with $\varepsilon < 0$ and investigate how the change in the sign of σ_a affects the pattern formation process with special emphasis on the $(--)$ case.

II.   EXPERIMENTAL SETUP AND MATERIALS

The experiments have been carried out on 4 homologs of the series *4-n-alkyloxy-phenyl-4-n'-alkyloxy-benzoates*:

where n and m denote the number of the carbon atoms of the terminal chains. We use the notation *n/m* to refer to the specific homologs with phase sequences as follows:

5/8: isotropic-85 ^{o}C-nematic-48 ^{o}C-crystalline

8/7: isotropic-88 ^{o}C-nematic-69.5 ^{o}C-smecticC- 62 ^{o}C- crystalline

10/4: isotropic-88.5 ^{o}C-nematic-79.6 ^{o}C-smecticA-(60 ^{o}C-smecticC)-64.5 ^{o}C-crystalline.

10/6: isotropic-89.5 ^{o}C-nematic-82 ^{o}C-smecticA-77.5 ^{o}C-smecticC-(43.5 ^{o}C-smecticB-30 ^{o}C-

2

crystalline2)-63$°C$-crystalline1, where () indicates monotropic transitions observed on cooling only.

All 4 substances have nematic phase which is followed on cooling by crystalline for **5/8**, by S_C for **8/7** and by S_A phase for **10/4** and **10/6**.

Ready-made 11μm cells (E.H.C. CO., Ltd.) have been used in the conventional sandwich geometry. The alignment was planar with the director parallel to the x direction. The SnO_2 transparent coating has been used as electrode to apply the electric field across the sample along the z direction.

The sample was placed into a thermostatted oven and an electromagnet with $\mathbf{H}||z$ and connected to a 4 terminal impedance bridge in order to measure the electrical properties σ_{ij} and ε_{ij} as a function of temperature. These measurements were carried out on the same samples used for the EC investigations in order to assure a correct *in situ* parameter determination.

The perpendicular components ($\varepsilon_\perp$ and $\sigma_\perp$) have been measured in the absence of the magnetic field ($H = 0$). Then H was increased and the complex impedance has been detected as a function of H. Since the cells are relatively thin a finite magnetic field does not result in a complete realignment of the director therefore $\varepsilon_\|$ and $\sigma_\|$ have been extracted by extrapolation of the magnetic field dependence of the capacity and the conductivity [17], respectively. The results are compared with those in [18–21] obtained using a cell thickness of about 1mm, which minimizes the effect of misalignment at the boundaries.

For providing the temperature control at the electroconvection measurements an Instec hotstage has been used. The patterns have been observed with a Leica polarizing microscope by using either the conventional shadow graph (single polarizer) technique [22] or two crossed polarizers. The images have been recorded by a CCD camera connected to a frame grabber card. The images have been stored with a resolution of 576×768 pixels and a 24 bit color depth then converted to 8 bit grayscale images for further processing.

III.   EXPERIMENTAL RESULTS

A.   Anisotropy of the electric properties

Figures 1a-d show the temperature dependence of ε_a of the homologs **5/8**, **8/7**, **10/4** and **10/6**, respectively, as the function of the relative temperature $T^* = (T - T_N)/(T_{NI} - T_N)$, where T_{NI} is the clearing point and T_N is the lower temperature limit of the nematic range. In the nematic range ($0 < T^* < 1$) ε_a is negative for all four homologs and becomes zero at T_{NI} ($T^* = 1$).

In the Figs. 1a-d we show the recent experimental results (open circles) together with literature data. Triangles represent another unpublished dataset obtained in our laboratory some time ago by using thin cells with and without magnetic field but not correcting $\varepsilon_\|$ for the incomplete realignment [23]. As expected the present measurements show a higher value of $|\varepsilon_a|$ than the uncorrected ones and it agrees well with the literature data (where available) in which thick cells were used [18–21]. The satisfying agreement is illustrated in Figs. 1b and 1d with the largest deviation around 15% with the exception of the one point of [24].

While the qualitative temperature behavior of ε_a is similar for the four homologs, $\sigma_a(T^*)$ varies strongly for the different materials as illustrated in Fig. 2 where the normalized conductivity anisotropy $\hat{\sigma}_a = \sigma_a/\sigma_\perp$ is plotted as a function of T^*.

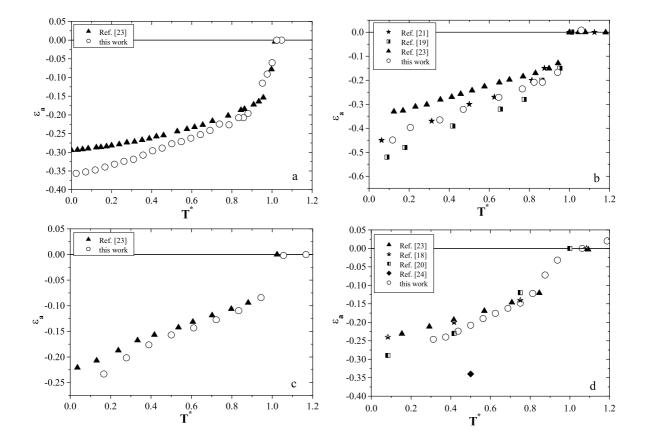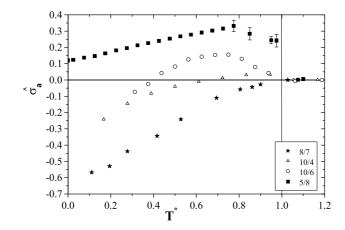We must emphasize the importance of the use of the normalized conductivity anisotropy: the

3

Figure 1: The dielectric anisotropy $\varepsilon_a = \varepsilon_\parallel - \varepsilon_\perp$ of 5/8 (a), 8/7 (b), 10/4 (c) and 10/6 (d) as a function of the relative temperature $T^* = (T - T_N)/(T_{NI} - T_N)$, where T_{NI} is the clearing point and T_N is the lower temperature limit of the nematic range.
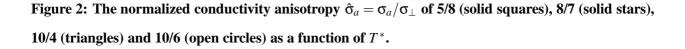
absolute value of σ_a may vary due to the impurities contaminating the cell during the filling procedure or aging, but $\sigma_a/\sigma_\perp$ is characteristic for the material.

The compound **5/8** has positive conductivity anisotropy in its whole nematic range (solid squares in Fig. 2). Its conductivity anisotropy slightly increases with temperature, then goes to zero at the T_{NI} phase transition point, as expected. In the vicinity of T_{NI} ($T^* > 0.75$) a larger scattering of the conductivity is observed than in the range of $T^* < 0.75$.

For the **8/7** the sign of $\hat{\sigma}_a$ is manifestly negative in the whole nematic range, it increases with increasing temperature and becomes zero at T_{NI} (see solid stars in Fig. 2). Our results reproduce the literature data [19], especially in the middle of the nematic range ($0.3 < T^* < 0.7$) where the difference is about 5%. For lower temperatures $T^* < 0.3$ the difference increases up to 18% (the anisotropy is larger in our case).

The conductivity anisotropy of **10/6** and **10/4** is illustrated by the open circles and triangles, respectively in Fig. 2. For both compounds $\hat{\sigma}_a$ has a sign inversion point below which the sign of the conductivity anisotropy is negative, above that point the sign turns into positive. The crossover is more pronounced for **10/6** (as already reported in Ref.[24]) while **10/4** has a shorter temperature range with $\hat{\sigma}_a > 0$ and the overshot is smaller as well. Comparing the data for **10/6** with Ref. [24]

4

Figure 2: The normalized conductivity anisotropy $\hat{\sigma}_a = \sigma_a/\sigma_\perp$ **of 5/8 (solid squares), 8/7 (solid stars), 10/4 (triangles) and 10/6 (open circles) as a function of** T^***.**

the qualitative behavior is similar. The sign inversion point is at the same temperature, however the magnitude of $|\hat{\sigma}_a|$ is significantly higher in our case (about 40% as a maximum).

The difference in the qualitative behavior of $\hat{\sigma}_a(T^*)$ between the 4 homologs presumably can be explained by their phase sequence. **5/8** does not have smectic phases (it crystallizes from the nematic) and its $\hat{\sigma}_a$ is positive in the whole nematic range as expected. In the 3 other homologs a smectic phase follows the nematic on cooling and pretransitional effects (formation of locally layered structures, i.e. the onset of quasi-smectic features with $\hat{\sigma}_a < 0$) lead to a strong decrease of $\hat{\sigma}_a$ with decreasing temperature and eventually to a negative $\hat{\sigma}_a$ [3, 19]. Whether this occurs already in the nematic range (**10/4** and **10/6**) or directly at T_{NI} (**8/7**) may depend on the type of the smectic phase (S_A for **10/4** and **10/6** and S_C for **8/7**) which follows the nematic on cooling or on the type of the phase transition (2nd order and 1st order, respectively).

From the combined behavior of $\varepsilon_a(T^*)$ and $\hat{\sigma}_a(T^*)$ one can predict the occurrence of EC patterns under the influence of an electric field in the four materials.

The material **5/8** is predicted to show EC in its whole nematic range since it belongs to the $(-+)$ category, hence we can compare the experimental results with the standard theory. Moreover the fit of the theory to the measured data (e.g. the frequency dependence of the EC threshold voltage U_c and that of the wavenumber $|\mathbf{q}_c|$ at onset) is an important tool to infer material parameters, such as the viscosity coefficients (α_i-s) difficult to measure directly.

In contrast to **5/8**, the material **8/7** belongs to the $(--)$ category hence it is prohibited to have spatially extended EC roll structures arising via a forward bifurcation as a primary instability in its whole nematic range.

The compounds **10/6** and **10/4** are appropriate to investigate how the sign of $\hat{\sigma}_a$ affects the pattern formation as it will be demonstrated in the next section.

5

B.   The properties of the patterns

An ac sinusoidal voltage U has been applied to the planarly aligned ($\mathbf{n}\|x$), thermostatted cells filled with the substances described above and the formation and evolution of patterns have been studied with a polarizing microscope. The control parameters are the dimensionless driving voltage $\varepsilon = \frac{U^2 - U_c^2}{U_c^2}$ where U_c is the EC threshold, the frequency f of the applied electric field and the temperature T.
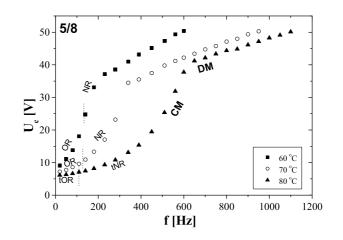

Figure 3: The EC threshold voltage U_c for 5/8 as a function of the frequency f at three different temperatures. CM, DM, NR, OR, tNR and tOR denote the conductive mode, the dielectric mode, normal rolls, oblique rolls, travelling normal rolls and travelling oblique rolls, respectively. The vertical dotted lines denote the Lifshitz points.

(i) 5/8. **5/8** shows conventional EC, which agrees well with the standard model worked out for $(-+)$ materials (and working well also for $(+-)$). Figure 3 shows the phase diagram, $U_c(f)$, at three different temperatures. Both the conductive (CM) and the dielectric modes (DM) with a crossover at the frequency f_c (where the 2 modes meet and their thresholds intersect) were observable in the whole temperature range. Henceforth we concentrate on the CM and carry out the theoretical fit for this range. As it is shown in Fig. 3 at onset we observe stationary oblique (OR) and normal rolls (NR) at $60°C$ ($T^* = 0.32$) and $70°C$ ($T^* = 0.59$) and travelling rolls (tOR and tNR) at $80°C$ ($T^* = 0.86$). The Lifshitz point (the frequency that separates the NR and OR range) slightly shifts towards lower frequencies with increasing temperature. This shift is more pronounced on the relative frequency scale (f/f_c).

Figures 4a,b show the quantitative comparison of the dependence of the experimental data obtained at $80°C$ ($T^* = 0.86$) on frequency of the threshold voltage U_c and that of the critical wavenumber $|\mathbf{q}_c| = \sqrt{q_x^2 + q_y^2}$ with the results of the linear stability analysis of the standard nemato-hydrodynamic description evaluated by a numerical Galerkin procedure [25]. The quantities used in the figures are $\omega = 2\pi f$ and the charge relaxation time $\tau_0 = \varepsilon_0 \frac{\varepsilon_\perp}{\sigma_\perp}$. The parameters $\varepsilon_\perp = 5.04$, $\varepsilon_\| = 4.79$, $d = 10.5 \mu m$ and $\hat{\sigma}_a = \sigma_a / \sigma_\perp = 0.33$ have been measured
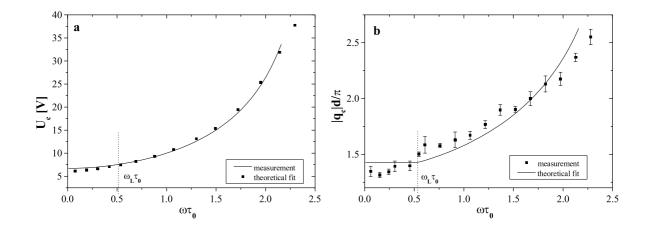
6

Figure 4: Comparison of the measured data (squares) and the linear stability fit (solid line) of the dependence of the threshold voltage U_c (a) and the critical wavenumber $|\mathbf{q}_c| = \sqrt{q_x^2 + q_y^2}$ (b) on $\omega\tau_0$ for 5/8, where $\omega = 2\pi f$ and $\tau_0 = \varepsilon_0 \frac{\varepsilon_\perp}{\sigma_\perp}$ is the charge relaxation time. The dotted line marks the Lifshitz point. The experiments were carried out at $80°C$ ($T^* = 0.86$).

and used for the calculations, the others were chosen in order to get a good fit for $U_c(\omega\tau_0)$ and $|\mathbf{q}_c|(\omega\tau_0)$ including the Lifshitz point [26]. This yielded $\alpha_1 = -18.1cp$, $\alpha_2 = -100.4cp$, $\alpha_3 = -1.1cp$ $\alpha_4 = 60.6cp$, $\alpha_5 = 70.9cp$, $\alpha_6 = -30.6cp$ as viscosities and $K_{11} = 6.1 \times 10^{-12}N$, $K_{22} = 2.7 \times 10^{-12}N$, $K_{33} = 8.61 \times 10^{-12}N$ as elastic constants. As demonstrated in Figs. 4a,b the compound **5/8** is well described even quantitatively by the standard theory with typical material parameters just slightly differing from those of MBBA [5].

(ii) 10/6. The change of sign of $\hat{\sigma}_a$ with temperature (at $T = 85°C$ $T^* = 0.4$) leads to a twofold character in the pattern formation of **10/6** as the substance shifts from category $(-+)$ to category $(--)$. Thus with decreasing temperature one expects a switching from the patterning electroconvecting state based on the Carr-Helfrich mechanism to a nonpatterning one [3, 5].

This crossover is not expected to occur precisely at $\hat{\sigma}_a = 0$, instead at a finite, positive $\hat{\sigma}_a^c$. It can be obtained from the expression determining the linear EC threshold U_c in the limit of large $|\mathbf{q}_c|$ (Eq. 4.1 in [5]), which diverges when $\hat{\sigma}_a$ decreases and reaches $\hat{\sigma}_a^c$. This occurs when A in the Eq. (3.1) goes to zero.

$$A = \omega^2 - \frac{\sigma_{||}}{\varepsilon_0^2 \varepsilon_\perp} \left[\frac{|\alpha_2|}{\eta_1} \left(\frac{\sigma_{||}}{\varepsilon_{||}} - \frac{\sigma_a}{\varepsilon_a} \right) - \frac{\sigma_\perp}{\varepsilon_{||}} \right], \tag{3.1}$$

where $\eta_1 = \frac{1}{2}(-\alpha_2 + \alpha_4 + \alpha_5)$.

For $\omega\tau_0 = 0$ one gets $\hat{\sigma}_a^c = \hat{\varepsilon}_a \left(1 - \frac{\eta_1}{|\alpha_2|}\right)$, where $\hat{\varepsilon}_a = (\varepsilon_{||} - \varepsilon_\perp)/\varepsilon_\perp$. Assuming that viscosities do not change dramatically with temperature in the middle of the nematic range we take the material parameters obtained by the comparison between the result of the theoretical linear stability analysis and the experimental data (see later) at $T^* = 0.8$ and the measured ones for the dielectric

7

permittivities for $T^* = 0.4$. We obtain $\hat{\sigma}_a^c = 0.012$, thus we expect the vanishing of the EC pattern (divergence of U_c) on cooling at $T^* = 0.41$ instead of $T^* = 0.40$.

The critical $\hat{\sigma}_a^c$ depends on the frequency of the applied ac voltage. For higher frequencies a higher $\hat{\sigma}_a^c$ is needed to preserve the EC pattern, namely $\hat{\sigma}_a^c$ is a monotonically increasing function of frequency, or *vice versa*, at a given $\hat{\sigma}_a$ the EC state is stable only below a *critical frequency* ω^c. Standard EC (s-EC) is expected above the line. With decreasing temperature, thus with decreasing $\hat{\sigma}_a$ in the range $T^* < 0.7$, the critical frequency reaches zero and the system is not expected to show any classical EC pattern. Consequently the standard EC state is limited in temperature from below and in frequency from above, thus one has a stability line $\hat{\sigma}_a^c$ versus $\omega\tau_0$ shown in Fig. 5 derived from Eq.1 using the material parameters of **10/6**.
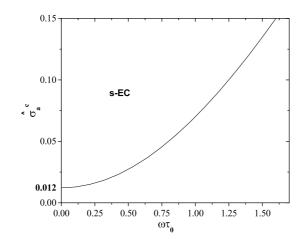

Figure 5: Calculated $\hat{\sigma}_a^c$ versus $\omega\tau_0$ above which the standard EC (s-EC) state exists for 10/6.

Although below the existence line the system is prohibited to show s-EC, we have found another convective pattern formation, which can not be explained by the conventional Carr-Helfrich mechanism, thus we call it non standard EC (ns-EC) [31].

In the following we first present the results related to the s-EC patterns then the observations of the ns-EC regime will be reviewed.

Within the existence region of s-EC for $T \geqq 88°C$ $(T^* \geqq 0.8)$ a spatially extended pattern occurs as usual normal or oblique rolls in almost the whole frequency range (the ns-EC range beyond the critical frequency ω^c would require such high voltages, which might destroy the cell). At lower temperature $(86°C < T < 88°C$ $(0.53 < T^* < 0.8))$, where $\hat{\sigma}_a$ is still positive and is above $\hat{\sigma}_a^c$ domains of normal rolls, travelling oblique rolls and a grid pattern (crossed oblique rolls) occur at $\omega < \omega^c$ under conditions similar to those in Ref. [24]. All these structures are observable with the conventional shadowgraph technique.

In this region **10/6** is expected to follow the predictions of the standard theory. Figures 6a,b show the result of the theoretical linear stability analysis and the experimental data taken at $88°C$ $(T^* = 0.8)$. For the calculation we used the measured parameters $\varepsilon_\perp = 4.27$, $\varepsilon_\parallel = 4.14$, $d = 10.5\mu m$ and $\hat{\sigma}_a = \sigma_a/\sigma_\perp = 0.17$. The rest were chosen in order to get the best simultaneous fit for $U_c(\omega)$ and $|\mathbf{q}_c|(\omega)$, which yielded $\alpha_1 = -9.8cp$, $\alpha_2 = -100.4cp$, $\alpha_3 = 1.1cp$, $\alpha_4 = 66.6cp$, $\alpha_5 = 79.9cp$, $\alpha_6 = -20.6cp$, $K_{11} = 6.1 \times 10^{-12}N$, $K_{22} = 2.7 \times 10^{-12}N$ and $K_{33} = 8.0 \times 10^{-12}N$. The parameters basically are close to those of **5/8** with an exception of α_3. The opposite sign of α_3 may be
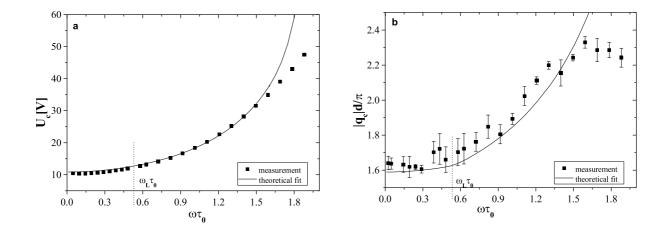
8

Figure 6: Comparison of the measured data (squares) and the theoretical predictions (solid line) for the dependence of the threshold voltage U_c (a) and the critical wavenumber $|\mathbf{q}_c| = \sqrt{q_x^2 + q_y^2}$ (b) on $\omega\tau_0$, for 10/6 at $88°C$ ($T^* = 0.8$). The dotted line denotes the Lifshitz point.

due to the influence of the smectic phase preceding the nematic phase for **10/6** (and not for **5/8**). The influence of the smectic phase on the viscosities is a known phenomenon, and discussed in [27, 28]. With these parameters the standard model provides a satisfactory quantitative description of the onset of s-EC patterns in **10/6** as demonstrated in Figs. 6a,b, with the exception of the high frequency range ($\omega\tau_0 \gtrsim 1.6$) where the measured data significantly deviate from the theoretical curve. These deviations are the consequence of the occurrence of ns-EC and will be discussed in more details below.

At high frequencies and low temperatures where no s-EC is expected we observed a new, spatially extended ns-EC structure not reported in [24].

The ns-EC structure shows some morphological similarities to the rolls of the standard EC, i.e. they exhibit as stripes of dark and light regions as demonstrated in Fig. 7a, which shows a snapshot obtained at $85°C$ ($T^* = 0.4$). The direction of the stripes, however, is unusual: it is basically parallel to the director (yielding *parallel stripes*, PS) or makes a small angle with it (*OS, oblique stripes*). In the following we review the properties of the ns-EC structure:

1. Director configuration, visibility and/or contrast. In addition to the unusual orientation of the stripes (PS) the pattern is weak, the overall contrast is low as compared to the s-EC structure. Near the onset of PS the pattern is not visible in the conventional shadow-graph method, crossed polars are needed to detect it. Thus the director field has no z component, i.e the director is modulated in the xy plane. This also explains the low contrast. The measurements were carried out with a polarizer parallel to the director and an analyzer perpendicular to that, which gave the best image quality and highest contrast. The voltage range where the PS structure is stable is wide in comparison with s-EC since it may persist up to $\varepsilon \approx 3$. These features are characteristic for PS in the whole frequency and temperature range. At higher ε (of the order of 1) the pattern becomes visible with a single polar i.e. the director tilts out of the xy plane. With further increase of ε local structures similar to the butterflies reported in Ref. [24] occur and coexist with the stripes.

2. The manner of the onset. The onset of the pattern is somewhat different from that of the
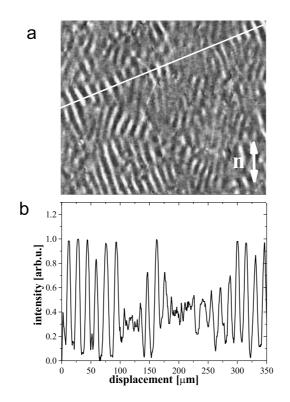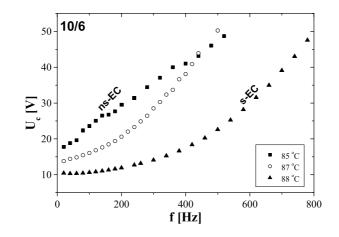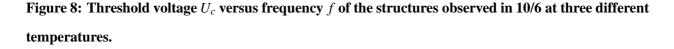
9

Figure 7: Snapshot of the ns-EC structure (oblique stripes, OS, see the text for description) taken with crossed polarizers (a) and the corresponding intensity profile (b) along the white line for 10/6 at $T = 85°C$ $(T^* = 0.4)$**,** $f = 100Hz$ $(\omega\tau_0 = 0.42)$ **and** $\varepsilon = 0.32$**. The director is vertical as it is shown by the white arrow and it is parallel to one of the crossed polarizers.**

standard EC rolls. The PS (or OS) sets in locally continuously in the form of patches extending over several stripes, which are separated by non-convecting regions. Above the onset the total picture is dynamic, convecting and non-convecting patches interchange. This structure fills the cell (i.e. no definite fronts exist that would separate the cell into distinct areas with and without pattern). The length of the stripes is finite and the amplitude is spatially inhomogeneous. Figures 7a,b demonstrates this inhomogeneity at $f = 100Hz$ $(\omega\tau_0 = 0.42)$ and $\varepsilon = 0.32$. Figure 7b shows the intensity profile along the white line in Fig. 7a perpendicular to the stripes.

On the other hand, at a given location the amplitude of the structure continuously increases with the voltage (locally no abrupt jump occurs). The transition from the quiescent state to the convective one is not sharp, the contrast grows slowly with the voltage performing a supercritical bifurcation.

3. Threshold, critical wavenumber and obliqueness. The further properties of the patterns differ fundamentally between s-EC and ns-EC. Figure 8 illustrates the difference in the behavior of U_c: at $88°C$ $(T^* = 0.8)$ (s-EC) over a large frequency range the threshold curve $U_c(f)$ follows the standard model up to $f \approx 600Hz$ $(\omega\tau_0 \approx 1.6)$. As can be seen, for higher frequencies the appearance of s-EC is preceded by the onset of ns-EC (see also Fig. 6a). This effect is more

10

Figure 8: Threshold voltage U_c versus frequency f of the structures observed in 10/6 at three different temperatures.

significant at $87°C$ $(T^* = 0.66)$ where the system shows a grid pattern (crossed oblique rolls) at threshold and follows the standard theory for $f < 300Hz$ $(\omega\tau_0 < 1)$, above which one has ns-EC (OS). At $85°C$ $(T^* = 0.4)$ one has ns-EC over the whole frequency range and the threshold increases linearly with frequency. On further cooling but remaining in the nematic phase the PS (or OS) structure persists for $\hat{\sigma}_a < 0$. In the region $82°C < T < 84°C$ $(0 < T^* < 0.4)$, however, the contrast of the pattern becomes lower when approaching the smectic phase. For observation of ns-EC at $\hat{\sigma}_a < 0$ the material **8/7** turned out to be more appropriate since it has $\hat{\sigma}_a < 0$ (and shows ns-EC) in its whole temperature range.
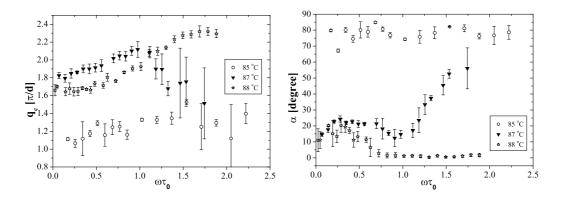

Figure 9: The dependence of the critical wavenumber $|\mathbf{q}_c| = \sqrt{q_x^2 + q_y^2}$ and the obliqueness $\alpha = \arctan\left(\frac{q_x}{q_y}\right)$ on $\omega\tau_0$ for 10/6 at $85°C$ $(T^* = 0.4)$, $87°C$ $(T^* = 0.66)$ and $88°C$ $(T^* = 0.8)$.

The different character of the s-EC and ns-EC structures and the presence of a critical point in frequency separating the two patterns are also captured in the critical wavenumber $|\mathbf{q}_c(\omega\tau_0)|$

11

and obliqueness $\alpha(\omega\tau_0)$ describing the angle between the wavevector $\mathbf{q}$ and the director $\mathbf{n}$ ($\alpha = \arctan(\frac{q_y}{q_x})$) as demonstrated at three different temperatures in Figs. 9a,b.

At $88°C$ ($T^* = 0.8$) $|\mathbf{q}_c(\omega\tau_0)|$ and $\alpha(\omega\tau_0)$ follow the predictions of the standard theory up to $\omega\tau_0 = 1.6$, as already shown in Fig. 6b. The system has a Lifshitz point at $\omega_L\tau_0 = 0.66$ which is slightly above the one provided by the linear theory ($\omega_L\tau_0$=0.56). The transition from s-EC to ns-EC at $\omega\tau_0 = 1.6$ is continuous thus the pattern at threshold preserves the NR character for higher frequencies though its regularity decreases by breaking up into slightly tilted patches forming the OS structure, and the two patterns coexist. Hence we observe a decrease in $|\mathbf{q}_c|$ and a slight increase in α above $\omega\tau_0 = 1.6$ as expected for ns-EC. For $87°C$ ($T^* = 0.66$) the onset wavenumber $|\mathbf{q}_c(\omega\tau_0)|$ has a maximum at $\omega\tau_0 \approx 1$ that separates the s-EC (grid pattern, lower frequency) from ns-EC (OS, higher frequency), (see solid down triangles in Fig. 9). The behavior of α also indicates the occurrence of a new structure by a sharp change in slope at $\omega\tau_0 \approx 1$. This is clearly visible despite the larger scattering of data due to the lower regularity of the ns-EC structure. The critical frequency at which $|\mathbf{q}_c|$ has a maximum and α has a break shifts to lower frequencies with decreasing temperature and below $86°C$ ($T^* = 0.53$) the system shows only ns-EC patterns. At $85°C$ ($T^* = 0.4$) (open circles in Fig. 9) the wavenumber and α are independent of frequency within the error bar. It is also seen that the direction of the stripes strongly turns with cooling, α is zero at high T and reaches $90°$ around $84°C$ ($T^* = 0.4$) so the stripes become practically parallel to the initial director.

In summary, the critical frequency decreases with decreasing temperature. At $T = 86°C$ ($T^* = 0.53$) where $\hat{\sigma}_a$ is still definitely positive solely PS (and OS) is seen. Above this temperature the material exhibits twofold behavior (s-EC, ns-EC), below this point only the non-standard EC pattern occurs as a primary instability. The qualitative behavior agrees well with the prediction obtained by the analysis of Eq. 3.1 i.e. at larger frequencies larger $\hat{\sigma}_a$ is needed (hence larger temperature) to preserve the stability of the NR regime.

In the experiments, however, the ns-EC structure takes over when its threshold becomes lower than the threshold of s-EC (namely when the two threshold curve cross over each other), which happens at a finite voltage. This means that with decreasing temperature s-EC is replaced by ns-EC at a $\hat{\sigma}_a > \hat{\sigma}_a^c$.

(iii) 10/4. The behavior of the substance **10/4** is qualitatively similar to that of **10/6**, thus it shows ns-EC when s-EC looses stability, which happens at $T \approx 85°C$ ($T^* \approx 0.6$) below which only PS (OS) is seen. At a given temperature it has also a critical frequency separating s-EC and ns-EC and it shifts towards lower frequencies with decreasing temperature.

Due to the shorter $\hat{\sigma}_a > 0$ range and significantly lower value of $\hat{\sigma}_a$ this substance is less appropriate for measurements, therefore no quantitative results of EC measurements will be presented here. Despite this, the qualitative agreement of the behavior indicates that the PS (or OS) structure is not unique and it is not solely characteristic for **10/6**.

(iv) 8/7. Since the material **8/7** has negative $\hat{\sigma}_a$ in its whole nematic range it is not expected to show conventional EC, instead ns-EC is observed.

The threshold of the PS (or OS) structure behaves similarly to that of the **10/6** namely it grows linearly with frequency. Figure 10 shows the threshold of the ns-EC structure at three different temperatures at $T = 72°C$ ($T^* = 0.14$) solid squares, at $T = 78°C$ ($T^* = 0.46$) open circles and at $T = 84°C$ ($T^* = 0.78$) solid triangles. For the two lower temperatures the direction of rolls is basically parallel to the director whereas for the latter case the obliqueness of the stripes increases from about $40°$ up to $80°$ with increasing frequency. Due to the lower regularity and low contrast of the ns-EC pattern the experimental wavenumber has a relatively large scattering around 1.3.
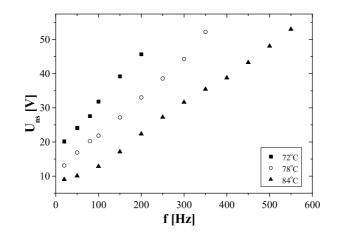
12

Figure 10: The threshold as a function of the frequency $U_c(f)$ **for 8/7 at** $T = 72°C$ $(T^* = 0.14)$**,** $T = 78°C$ $(T^* = 0.46)$ **and** $T = 84°C$ $(T^* = 0.78)$**.**

Without going into details we mention that besides the PS and OS structures with increasing ε a great variety of other structures occur, namely star-like local structures existing alone or coexisting with the primary PS (or OS) structure, or NR takes place as a secondary instability. Studies of these structures are in progress.

IV.   SUMMARY

We have studied four homologs with different phase sequences. We measured the anisotropy of the dielectric permittivity ε_a and the normalized conductivity $\hat{\sigma}_a = \frac{\sigma_a}{\sigma_\perp}$ as a function of temperature. The compound **5/8** has negative dielectric anisotropy and positive conductivity anisotropy in its whole nematic range while for **8/7** both of these properties are negative. The materials **10/6** and **10/4** have negative ε_a and a sign inversion temperature of their conductivity $\hat{\sigma}_a$. Using these four materials we investigated the influence of the sign of $\hat{\sigma}_a$ on the EC pattern formation.

Comparison between the prediction of the linear stability analysis of the standard nemato-hydrodynamic description of EC and the experimental data were carried out for the compounds **5/8** and **10/6** and good agreement was found. (Although **10/4** has a similar qualitative behavior like **10/6** it was less appropriate for measurements.) The analysis of the expression determining the linear EC threshold in the limit of large $|\mathbf{q}|$ a finite positive $\hat{\sigma}_a^c$ was found at which the standard EC disappears. As it also turned out this critical $\hat{\sigma}_a^c$ is a monotonically increasing function of the frequency of the driving ac voltage.

Additionally to the well-known patterns of the s-EC we found new structures which can not be described by the standard EC model (ns-EC, [31]). This patterns show morphological similarity to the normal and oblique rolls as they show up as stripes with a direction mostly parallel to the initial director (PS) or they can be oblique (OS). The new structures take place at low temperature and thus at low $\hat{\sigma}_a$ when the threshold of the s-EC structure becomes higher than that of ns-EC. This occurs at a finite positive $\hat{\sigma}_a$ and PS (or OS) persist also for negative conductivity anisotropies.

13

The formation of the PS (or OS) cannot be described by the Carr-Helfrich (anisotropic) mechanism therefore an isotropic effect is probably responsible. The *injection mode* can presumably be excluded due to its strongly non-linear threshold $U_c(f)$ while the *electrolytic mode* [29, 30] is a more probable candidate due to the similarity in the threshold behavior.

More detailed studies of the ns-EC structure are in progress, such as the investigation of the non-linear behavior above threshold included secondary instabilities and the dynamics of the patterns, with special emphases on the vicinity of the isotropic phase transition.

ACKNOWLEDGEMENTS

[1] M. C. Cross and P. C. Hohenberg, Rev. Mod. Phys **65**, 851 (1993).

[2] J. P. Gollub and J. Langer, Rev. Mod. Phys. **71**, S396 (1999).

[3] P. G. de Gennes, *The Physics of Liquid Crystals* (Clarendon Press, Oxford, 1974), 2nd ed.

[4] L. Kramer and Á. Buka, eds., *Pattern Formation in Liquid Crystals* (Springer-Verlag, New York, 1996).

[5] E. Bodenschatz, W. Zimmermann, and L. Kramer, J. Phys. France **49**, 1875 (1988).

[6] S. Nasuno, O. Sasaki, and S. Kai, Phys. Rev. A **46**, 4954 (1992).

[7] J. H. Huh, Hidaki, and S. Kai, Phys. Rev. E **58**, 7355 (1998).

[8] S. Rudroff, V. Frette, and I. Rehberg, Phys. Rev. E **59**, 1814 (1990).

[9] E. Plaut, W. Decker, A. Rossberg, L. Kramer, and W. Pesch, Phys. Rev. Lett. **79**, 2367 (1997).

[10] R. Ribotta and A. Joets, Phys. Rev. Lett. **56**, 1595 (1986).

[11] M. de la Torre Juarez and I. Rehberg, Phys. Rev. A **42**, 2096 (1990).

[12] M. Treiber, N. Éber, Á. Buka, and L. Kramer, J. de Physique II (Paris) **7**, 649 (1997).

[13] M. Dennin, D. S. Cannel, and G. Ahlers, Phys. Rev. E **57**, 638 (1998).

[14] D. Funfschilling, B. Sammuli, and M. Dennin, Phys. Rev. E **67**, 016207 (2003).

[15] Á. Buka, B. Dressel, W. Otowski, K. Camara, T. T´oth-Katona, L. Kramer, J. Lindau, G. Pelzl, and W. Pesch, Phys. Rev. E **66**, 051713 (2002).

[16] B. Dressel and W. Pesch, Phys. Rev. E **67**, 031707 (2003).

[17] H. Deuling, *Elasticity of nematic liquid crystals* (Academic Press, Inc. Kassel, Germany, 1978), ISBN 0-12-607774-6, p. 77.

[18] Á. Buka, Mol. Cryst. Liq. Cryst. **49**, 159 (1979).

[19] J. Jadzyn and P. Kedziora, Mol. Cryst. Liq. Cryst. **145**, 17 (1987).

[20] H. Kresse and D. Demus, *Forschungen uber flussige kristalle* (Halle, 1983), p.59.

[21] H. Kresse, A. Wiegeleben, and D. Demus, Krist. Tech **34**, 15 (1980).

[22] S. Rasenat, G. Hartung, B. L. Winkler, and I. Rehberg, Exp. in Fluids **7**, 412 (1989).

[23] Z. V´aradi, Diploma thesis, BME (1998).

[24] H. R. Brand, C. Fradin, P. L. Finn, W. Pesch, and P. E. Cladis, Phys. Lett. A **235**, 508 (1998).

[25] E. Plaut and W. Pesch, Phys. Rev. E **59**, 1747 (1999).

[26] W. Zimmermann and L. Kramer, Phys. Rev. Lett. **55**, 402 (1985).

[27] H. Kneppe, F. Schneider, and N. Sharma, Ber. Bunsenges. Phys. Chem. **85**, 784 (1981).

[28] H. Kneppe, F. Schneider, and N. Sharma, J. Chem.Phys. **77(6)**, 3203 (1982).

[29] L. Blinov and V. Chigrinov, *Electrooptic Effects in Liquid Crystal Materials* (Springer-Verlag, New York, 1994).

[30] L. M. Blinov, Sci. Prog., Oxf. **70**, 263 (1986).

[31] By observing moving dust particles we detected periodic motion (fbw) in the plane perpendicular to the stripes similarly in both the s-EC and ns-EC cases, which is a direct indication of convection.